Density functional study of the magnetic coupling in $V(TCNE)_2$

Giulia C. De Fusco,[1] Leonardo Pisani,[1] Barbara Montanari,[2] and Nicholas M. Harrison[1,3]
[1]*Department of Chemistry-Thomas Young Centre, Imperial College London, South Kensington Campus, London SW7 2AZ, United Kingdom*
[2]*STFC Rutherford Appleton Laboratory, Chilton, Didcot, Oxfordshire OX11 0QX, United Kingdom*
[3]*STFC Daresbury Laboratory, Daresbury, Warrington WA4 4AD, United Kingdom*
(Received 2 December 2008; published 4 February 2009)

A simple model structure of the room-temperature magnetic semiconductor $V(TCNE)_2$ is proposed on the basis of available experimental data. The structural, electronic, and magnetic properties are investigated using hybrid-exchange density functional theory within periodic boundary conditions. A spin-polarized ferrimagnetic ground state with a total spin of $1\mu_B$ per formula unit is identified. The analysis of the corresponding electronic band structure and spin distribution reveals strong interactions between the V ions and the $[TCNE]^{\cdot-}$ radicals, identified as spin carrying units. Within a simple Ising Hamiltonian, a strong antiferromagnetic coupling between the metal and its nearest-neighbor ligands is predicted which is consistent with the observed high-temperature magnetic ordering. The computed results provide useful insight into the physical origin of the exceptional magnetic behavior of $V(TCNE)_2$.

DOI: 10.1103/PhysRevB.79.085201 PACS number(s): 75.50.Xx, 75.50.Gg, 71.23.Cq, 71.15.Mb

I. INTRODUCTION

In the past two decades organic and molecular magnets have received increasing attention due to their specific properties which make them attractive candidates for many technological applications. Compared to conventional metallic and ceramic magnets, this class of materials offers several advantages. Among these are the modulation/tunability of their properties via organic methodologies, the low-temperature processability, and the possibility to combine magnetic, optical, mechanical, and electronic properties.[1,2] Materials based on transition-metal-tetracyanoethylene, *M*-TCNE (*M*=V, Mn, Fe, etc.[3–5]), complexes are of particular interest. These compounds exhibit a large range of relatively high critical temperatures and a rich magnetic behavior, including ferromagnets, ferrimagnets, canted/weak ferromagnets, and spin glasses. In this family of hybrid magnets, $V[TCNE]_x$ ($x\sim 2$) (Refs. 3, 6, and 7) represents a major breakthrough as it displays magnetic ordering above room temperature ($T_C\sim 400$ K).[8,9] A stoichiometry close to $V(TCNE)_2$ has been suggested from elemental analysis[3] and this composition has been recently confirmed by x-ray photoelectron spectroscopy (XPS) measurements, from which a nitrogen to vanadium ratio of $R_{NV}=7.5$ (Ref. 10) has been deduced.

This three-dimensional (3D) molecular-based material is a soft magnet with low coercive field[7,11] and exhibits room-temperature semiconducting behavior with a thermal activation energy of 0.5 eV.[12,13] Studies based on x-ray absorption near-edge spectroscopy (XANES) and XPS measurements have suggested that the oxidation state of V is near +2.[7,14] From saturation magnetization and x-ray magnetic circular dichroism (XMCD) results, it is found that V^{2+} ions are in the high spin state ($S=3/2$) and that $[TCNE]^{\cdot-}$ has net spin $S=1/2$ with one unpaired electron in the π^* orbital.[7,10] The coupling between the 3/2 spin on the V ion and the 1/2 spin on each $[TCNE]^{\cdot-}$ is proposed to be antiparallel, yielding a saturation moment of $\sim 1\mu_B$ per formula unit.[3,9] Moreover magnetotransport studies performed via magnetic characterization of solvent free films of $V(TCNE)_2$ with electron paramagnetic resonance (EPR) have shown an anomalous increase in resistance (positive magnetoresistance) with applied magnetic field, H, up to $\sim 0.7\%$ at $H=6$ kG, i.e., three orders of magnitude more than the value predicted for conventional disordered semiconductors.[12,15] The origin of this behavior has been explained in terms of charge transport involving hopping of electrons in the $[TCNE]^{\cdot-}\pi^*$ bands.[12,13,15] According to the charge hopping model, the half-filled π^* electronic $[TCNE]^{\cdot-}$ band is split by strong on-site Coulomb repulsion into two oppositely spin-polarized subbands, one occupied and one unoccupied, which leads to a half semiconducting behavior.

Due to the presence of spin-polarized charge carriers in $V(TCNE)_2$, many commercial applications have been envisaged, including spintronics (spin-based electronics[16–19]) and magnetic shielding.[20–22] In addition it has been shown that both the magnetic and electrical properties of the material can be controlled via optical excitations,[23,24] suggesting potential applications for magneto-optical devices. However, the commercial use of $V(TCNE)_2$ is currently limited as the material is amorphous and extremely air and water sensitive.[3,6,7,10,11] The lack of long-range order and the substantial influence of the synthetic procedure (i.e., starting materials,[3,25] solvent,[9] and preparation method[6,7,26,27]) on the system properties clearly suggest that $V(TCNE)_2$ compounds contain structural defects and impurities such as residual solvent and/or by-products. Furthermore, it is possible that multiple metastable structures are thermodynamically feasible under typical preparation conditions. Since x-ray diffraction (XRD) cannot be used to determine the structure of such a highly disordered material, no relationship has been established between the structural features and the electronic and magnetic properties. Nevertheless its local coordination environment has been determined from extended x-ray absorption fine structure (EXAFS) measurements.[14] These data indicate V–N sixfold coordination with average V–N distance of 2.076(4) Å (10 K) in a slightly distorted octahedral ge-

ometry. Further insight into the structure of $V(TCNE)_2$ can be provided by x-ray-determined structural features of ordered *M*-TCNE analogs such as $[MnTPP]^+[TCNE]^{\cdot-}$ (TPP =*meso*-tetraphenylporphinato) (Refs. 8 and 28) and $[Fe(TCNE)_2]\cdot z(CH_2Cl_2)$.[29] The first is a linear-chain ferrimagnet with Mn^{III} ions coordinated by four porphyrin nitrogens and two $[TCNE]^{\cdot-}$ nitrogens, forming an octahedral complex. Each $[TCNE]^{\cdot-}$ is *trans*-μ-bonded to two metal ions and connects the planar $[MnTPP]^+$ groups thus forming infinite one-dimensional (1D) chains. The latter is a magnet with T_C=97 K that has a complex magnetic behavior featuring a mixture of ferrimagnetic and random anisotropy characteristics.[5] Its structure, determined from synchrotron powder diffraction data, consists of layers of Fe^{II} ions and μ_4-$[TCNE]^{\cdot-}$ linked by μ_4-$[C_4(CN)_8]_2$ dimers. Each Fe^{II} is octahedrally coordinated to six N atoms: four from four different μ_4-$[TCNE]^{\cdot-}$ within a layer and two from the diamagnetic linkers. In a recent paper the experimental geometry of $[Fe(TCNE)_2]\cdot z(CH_2Cl_2)$ has been used as a starting point for a numerical study of its V analog (performed using the local spin-density approximation with on-site Coulomb interaction *U* density functional), which predicts a spin-polarized ferrimagnetic ground state with magnetization corresponding to $2\mu_B$ per formula unit.[30] The existence in *M*-TCNE compounds of $[TCNE]^{\cdot-}$ ligands with uncoordinated cyano groups, such as the $[C_4(CN)_8]_2$ dimers and the *trans*-$\{\mu-[TCNE]\}^{\cdot-}$ linkers described above, has been confirmed by infrared spectroscopy (IR) (Refs. 7, 29, and 31) and XPS studies.[10] More specifically, IR spectra obtained for $V(TCNE)_2$ exhibit multiple peaks for CN vibrations suggesting a variety of bonding configurations and/or the presence of different forms of reduced TCNE.[7] The geometric parameters and the spin distribution of isolated $[TCNE]^{\cdot-}$ in its planar geometry have been deduced from single-crystal polarized neutron diffraction (PND) studies of tetra-*n*-butylammonium tetracyanoethenide, $[Bu_4N]^+[TCNE]^{\cdot-}$.[32] These results have been used as a reference throughout this work.

The present work proposes a model structure for $V(TCNE)_2$ on the basis of the experimental evidence discussed above. The structural, electronic, and magnetic properties of this simple model are computed and compared to the available data. The energies of a number of low-lying magnetic states are calculated and used to parametrize a model Ising Hamiltonian. A detailed analysis of the electronic structure and the Mulliken spin distribution obtained for the model system provides valuable insights into the physical mechanism underlying the high-temperature magnetic behavior of $V(TCNE)_2$.

The paper is organized as follows. Section II describes the methodology employed. In Sec. III A a simple model structure of $V(TCNE)_2$ is presented and the computed geometric parameters are discussed. The ground-state electronic properties of the system are investigated in Sec. III B. In Sec. III C a set of selected spin states is reported in order to evaluate the strength of the exchange interaction in terms of calculated magnetic exchange coupling constants, *J*. The computed results are discussed in Sec. IV. The main conclusions of this study are summarized in Sec. V.

II. COMPUTATIONAL DETAILS

The calculations presented herein have been performed using the hybrid-exchange density functional in the B3LYP form[33–35] as implemented in the CRYSTAL06 package.[36] The mixing of nonlocal and semilocal exchange provides a reliable representation of the structural and electronic properties of strongly correlated electron systems.[37,38] Moreover this method has become a well established approach to calculate optical band gaps, magnetic moments, spin-density distributions, and magnetic coupling constants in strongly interacting systems yielding a quantitative description of molecular-based magnetic systems.[39–45] The CRYSTAL software is based on the expansion of crystalline orbitals (COs) as a linear combination of a local basis set consisting in a set of atom-centered Gaussian type functions.[46] An 86-411 G^* (one *s*, four *sp*, and two *d* shells) triple valence and 6-31 G^* contraction double valence (one *s*, three *sp*, and one *d* shells) quality basis sets have been selected to describe the vanadium atoms and the second period elements (carbons and nitrogens), respectively.[47] The same basis sets and numerical approximations have been used to perform calculations on the isolated TCNE and $[TCNE]^{\cdot-}$ molecules which have been adopted as reference systems for the organic ligand. The Pack-Monkhorst sampling[48] of the reciprocal space lattice has been carried out selecting a grid of shrinking factor equal to six (resulting in 112 *k* points in the IBZ). The truncation of the Coulomb and exchange series in direct space has been controlled setting the Gaussian overlap tolerance criteria to 10^{-7}, 10^{-7}, 10^{-7}, 10^{-7}, and 10^{-14}.[46] The self-consistent field iterative procedure has been converged to a tolerance in the total energy of $\Delta E=1\times10^{-7}$ a.u. per unit cell (p.u.c.). To accelerate convergence of the self-consistent field (SCF) process, all calculations have been performed adopting a linear mixing of 70% and Anderson second-order mixing scheme. Different spin configurations have been studied as metastable states generated by altering an initial wave function, obtaining converged self-consistent field solutions for each electronic spin distribution. The initial density matrix has been formed from a superposition of suitable atomic densities. Initial constrains on the total spin of the cell have also been used to generate metastable states; however all data reported are from unconstrained and self-consistent solutions.

III. RESULTS

A. Geometry and structural relaxation

A model of a V-TCNE structure sublattice which satisfies a set of constraints based upon experimental evidence has been developed. These constraints include (i) the observed stoichiometry $V(TCNE)_2$,[3,8,10] (ii) the suggested octahedral coordination for the metal ion,[14] (iii) the presence of uncoordinated cyano groups,[7,10,31] and (iv) the dimensionality of the material forming a periodic crystalline network of V atoms and TCNE molecules. The resulting structure consists of a rectangular planar array of V atoms and TCNE molecules which form bidimensional planes linked through parallel chains of *trans*-μ-bonded TCNEs. The same structural motifs have been experimentally observed for 1D

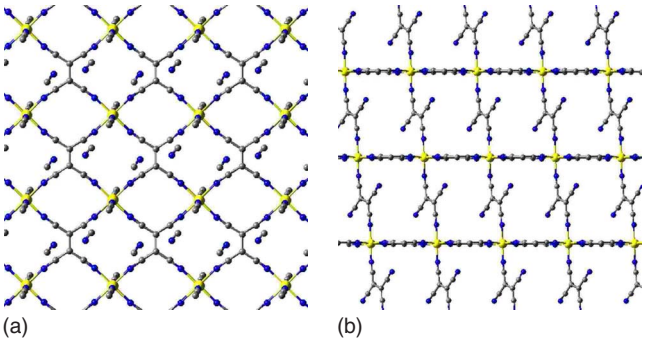

FIG. 1. (Color online) Schematic ball-and-stick representation of the optimized $V(TCNE)_2$ three-dimensional structure displayed (a) in the **ab** plane and (b) perpendicular to the **c** axis. The vanadium, carbon, and nitrogen atoms are represented as white (yellow online), gray, and black (blue online) balls, respectively.

[Mn(porphyrin)][TCNE]-based magnets[8] and $[Fe(TCNE)_2]$ compounds.[29] A local structure of $V(TCNE)_2$ with $\{V(\mu_4-[TCNE])^{-}\}$ layers interconnected by *trans*-$\{\mu-[TCNE]\}^{\cdot-}$ linkages has been previously suggested.[29] The structure proposed herein serves as a model system within which the material electronic and magnetic properties can be computed and analyzed. The geometric parameters of an isolated $[TCNE]^{\cdot-}$ ion, as determined from PND studies of $[Bu_4N]^+[TCNE]^{\cdot-}$, were taken as an initial geometry of the ligands.[32] After a full geometry optimization, a triclinic unit cell with lattice parameters **a**=7.266 Å, **b**=7.156 Å, **c**=9.971 Å, α=106.33°, β=98.16°, and γ=90.09° was obtained. Each unit cell contains one V atom at coordinates $(\frac{1}{2},\frac{1}{2},\frac{1}{2})$ and two organic ligands lying in the planes (0 0 1) and (1 1 0), hereinafter referred as equatorial TCNE and apical TCNE, respectively (Fig. 1). The metal is surrounded by six ligands in a slightly distorted octahedral coordination, with the smaller bond angle $N_{eq}-V-N_{eq}$ equal to 87.21°, and with the length of the four equatorial $V-N_{eq}$ bonds longer than the two apical $V-N_{ap}$ bonds. The optimized bond lengths (in Å) are 2.077(±0.002) for $V-N_{eq}$ and 2.070 for $V-N_{ap}$ in agreement with EXAFS measurements from which it is deduced that each vanadium ion is coordinated by 6.025 ± 0.25 nitrogen atoms at the average distance of 2.076(4)Å at 10 K.[14] The calculated geometric parameters of the equatorial and apical ligands are given in Table I. The computed ligand structure is consistent with that determined by PND for $[Bu_4N]^+[TCNE]^{\cdot-}$.[32] In addition, the relaxed atomic coordinates of the equatorial and apical ligands have also been compared to those obtained by optimizing isolated molecules of $[TCNE]^n$ (n=0,1−). As expected upon addition of one electron to a π^* molecular orbital (MO), a bond length increase with increasing negative charge is observed. The geometrical parameters of both ligands within the crystalline structure are comparable to the distances obtained for the free radical molecule, suggesting the presence of a unitary negative charge on the organic ligands as previously deduced from XPS and combined photoelectron spectroscopy (PES)/resonant photoemission (RPE) data.[10,26] The calculated Mulliken charge populations provide a further confirmation: the equatorial and apical ligands carry a negative charge of $-0.88|e|$ and $-0.87|e|$, respectively. The metal oxidizes transferring $\sim1.75|e|$ to the molecules, in agreement with the valence state deduced from XANES and XPS measurements.[7,10,14] Compared to the equatorial ligand whose four C–CN and four C≡N bonds all have the same bond lengths (as in the case of the isolated radical anion), the apical ligand shows two different single and triple bond distances. This difference is related to the inequivalent coordination environment of the cyano groups, two of which are σ-bonded to the V atoms while the remaining two are unbonded, in a trans configuration [Fig. 1(b)].

TABLE I. Calculated interatomic distances (Å) for isolated $[TCNE]^n$ (n=0,1−) and $[TCNE]^{\cdot-}$ within the 3D crystal lattice and crystallographically determined bond lengths for $[TCNE]^{\cdot-}$.

		$[TCNE]^{-}$		$V(TCNE)_2$	
Parameter (Å)	TCNE	exp[a]	calc	$[TCNE]^{-}_{eq}$	$[TCNE]^{\cdot-}_{ap}$
C–C	1.363	1.429(8)	1.432	1.436	1.443
C–CN	1.426	1.406(9)	1.405	1.401	1.396
		1.393(9)			1.417
		1.419(9)			
		1.405(9)			
C≡N	1.159	1.157(7)	1.167	1.169	1.170
		1.181(8)			1.168
		1.164(7)			
		1.177(7)			

[a]Determined from PND data on $[Bu_4N]^+[TCNE]^{\cdot-}$ (Ref. 32).

B. Electronic structure

The computed electronic band structure of the geometrically relaxed model is displayed in Fig. 2. The one-electron

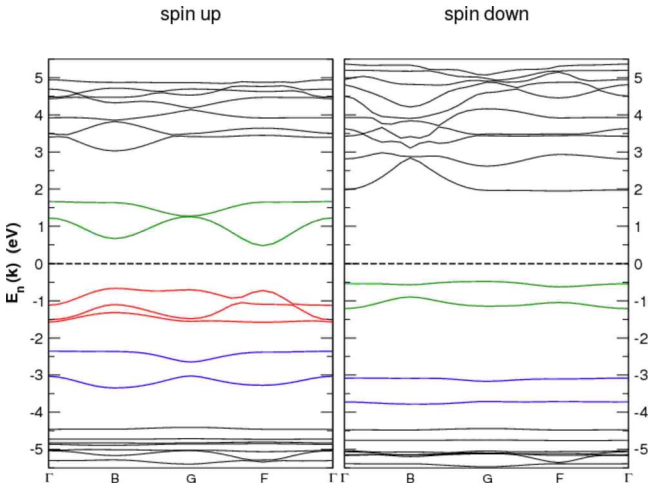

FIG. 2. (Color online) The electronic structure of $V(TCNE)_2$ in its ground-state antiferromagnetic (AFM) configuration. The energy scale (eV) has been normalized and expressed relatively to the Fermi energy, E_F. On the x axis the points labeled as Γ, B, G, and F correspond to the k points of the first Brillouin zone of the triclinic and monoclinic Bravais lattices whose absolute coordinates are (0,0,0), $(\frac{1}{2},0,0)$, $(0,0,\frac{1}{2})$, and $(0,\frac{1}{2},0)$, respectively.

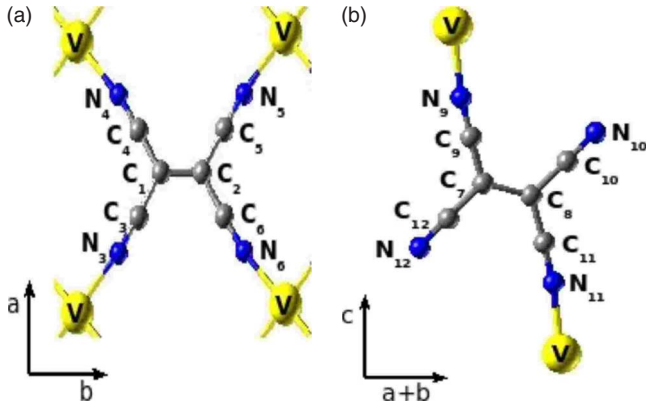

FIG. 3. (Color online) Ball-and-stick representation of the optimized $V(TCNE)_2$ formula unit as seen along (a) the **ab** plane and (b) the **c** axis. The vanadium, carbon, and nitrogen atoms are represented as white (yellow online), gray, and black (blue online) balls, respectively.

bands for spin-up (α) and spin-down (β) electrons are shown separately. A spin-polarized semiconducting behavior with an indirect spin-up band gap of 0.82 eV is predicted in reasonable agreement with the activation energy of conductivity reported by Prigodin *et al.*[12] ($\Delta E \simeq 0.5$ eV). In what follows a detailed analysis of the one-electron COs is used to clarify the magnetic coupling mechanism which results in the exceptional high-temperature ferrimagnetic behavior of the V-based material. The three upper α valence bands ($-1.60 \div -0.36$ eV; depicted in red in Fig. 2) are dominated by the V $3d$ states, d_{xz}, d_{yz}, and $d_{x^2-y^2}$, with some hybridization with $2p$ atomic orbitals (AOs) localized on six cyano carbons (C_3, C_4, C_5, C_6, C_9, and C_{11} in Fig. 3). At lower energies, between −3.40 and −2.37 eV, the two bands (in blue, on the left, in Fig. 2) have the predominant character of the ligand π electrons. As can be seen in Fig. 2, the same states contribute to the β valence bands in the energy range from −3.08 to −3.81 eV. Both the spin-up lower conduction states and the spin-down upper valence states are dominated by the two TCNEs π^* MOs (in green in Fig. 2). The nature of the frontier electronic structure can be characterized by means of spectroscopic studies. A combination of RPE, PES, and near-edge x-ray absorption fine structure (NEXAFS) has shown that the upper valence states are V ($3d$) derived, exhibiting a significant hybridization between V ($3d$) and TCNE cyano carbons, while the lower conduction states are dominated by the ligand singly occupied molecular orbital (SOMO), with no hybridization with V-related states.[10,49] The character of the computed COs is in excellent agreement with these findings. This provides indirect support for the essential features of the structure model adopted here. In addition, α and β valence states of hybrid V $3d$ (d_{xy} and d_{z^2}) and TCNE σ MOs character are found to lie between −8.23 and −7.80 eV. The corresponding antibonding σ^* states are located in the spin-polarized conduction bands in the energy range between 4.68 and 6.79 eV.

The Mulliken spin populations of $V(TCNE)_2$ and $[TCNE]^{\cdot-}$ free radical are reported in Table II. Experimental values obtained with single-crystal PND have also been given for comparison.[32] Both experimental and density functional data show that ~30% of the free radical total spin is localized on each vinyl carbon, ~−7% on a cyano carbon, and ~17% on a nitrogen atom. Related to these values, the calculated spin populations of the TCNE moieties of $V(TCNE)_2$ undergo several changes. In both ligands the spin-down population is redistributed between the central C's (C_1, C_2, and C_7, C_8 in Fig. 3) and the four N's with increasing contribution from the latter. The total spin (in absolute value) on the $[TCNE]^{\cdot-}$ moiety in $V(TCNE)_2$ is lower than that in free space. This is due to a general increase in the spin-up population localized on the cyano carbons. In addition the equatorial and the apical ligands show different spin populations (Table II) providing further evidence of the significant effect played by the environment on the spin distribution within the ligand. As in the isolated ion, in the equatorial $[TCNE]^{\cdot-}$ all atoms of the same atom type carry the same spin due to the identical coordination environment. Compared to the equatorial ligand, in the axial $[TCNE]^{\cdot-}$ the spin populations localized on C_9, C_{11}, N_9, and N_{11} (Fig. 3) do not show any remarkable variation while the spin densities of cyano carbons (C_{10} and C_{12} in Fig. 3) and nitrogens (N_{10} and N_{12}) belonging to the dangling CN groups show a substantial decrease. Moreover, there is an increase in the spin-down population of the two vinyl carbons (C_7,C_8). The spin-up and spin-down density blocks are shown separately in the spin-density maps in Fig. 4. In agreement with the Mulliken spin population data (in Table II) and the analysis of the upper valence COs, the isosurface for the spin-up charge density is mainly localized on the metal ion and the $[TCNE]^{\cdot-}$ cyano carbons. The overall shape of the isosurface localized on the V is consistent with the spin-density distribution expected for an octahedral complex with a t_{2g}^3 configuration.[50] The spin-density distribution of the cyano C's has the shape of a circular crown which can be consid-

TABLE II. Comparison of experimental spin populations ($|e|$) of $[TCNE]^{\cdot-}$ ion with density functional results obtained for an isolated $[TCNE]^{\cdot-}$ radical, and for the equatorial and apical $[TCNE]^{\cdot-}$ ligands within the crystalline structure. The labels assigned to each atom are referred to the structures represented in Fig. 3.

	$[TCNE]^{\cdot-}$		$V(TCNE)_2$		$V(TCNE)_2$
Atom	exp[a]	calc[b]	$[TCNE]^{\cdot-}_{eq}$	Atom	$[TCNE]^{\cdot-}_{ap}$
C_1	0.33	0.30	−0.25	C_7	−0.28
C_2	0.33	0.30	−0.25	C_8	−0.28
C_3	−0.05	−0.07	0.13	C_9	0.11
C_4	−0.04	−0.07	0.13	C_{10}	0.05
C_5	−0.03	−0.07	0.13	C_{11}	0.11
C_6	−0.08	−0.07	0.13	C_{12}	0.05
N_3	0.12	0.17	−0.16	N_9	−0.18
N_4	0.12	0.17	−0.15	N_{10}	−0.12
N_5	0.13	0.17	−0.16	N_{11}	−0.18
N_6	0.16	0.17	−0.15	N_{12}	−0.12
Total spin	0.99	1.00	−0.60		−0.82

[a]Determined from PND data on $[Bu_4N]^+[TCNE]^{\cdot-}$ (Ref. 32).
[b]Calculated for the optimized geometry of $[TCNE]^{\cdot-}$ radical in free space.

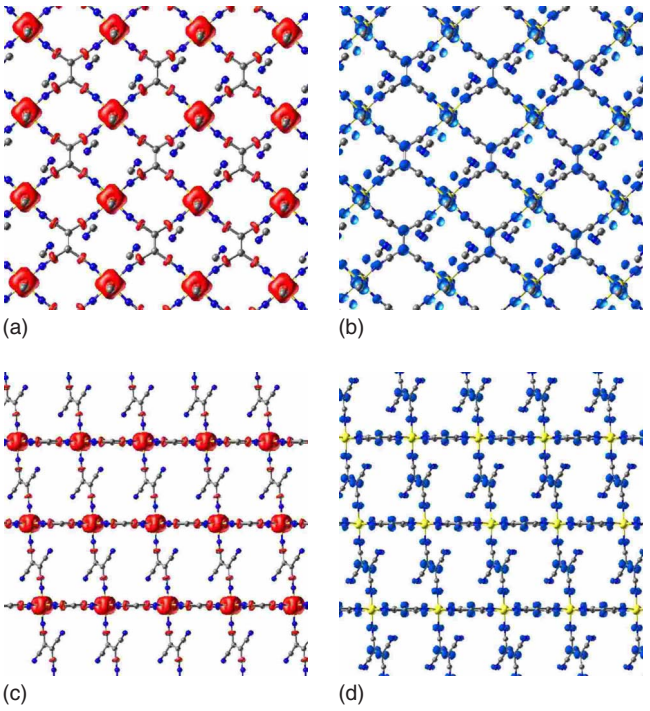

FIG. 4. (Color online) Spin-up and spin-down density maps of $V(TCNE)_2$ lowest total-energy state as seen along [(a) and (b)] the **ab** plane and [(c) and (d)] the **c** axis. The dark gray (red online) and black (cyan online) isosurfaces are $+0.007\mu_B/a_0^3$ and $-0.012\mu_B/a_0^3$, respectively.

ered as derived from the overlap of (p_x-p_y) and p_z AOs. No significant spin-up population is localized on the two apical cyano C's, C_{10} and C_{12}, belonging to the uncoordinated CN groups. The negative spin-density distribution is spread throughout the π^* system of the $[TCNE]^{\cdot-}$ ligands, mapping the shape of the SOMO: the spin density on the vinyl carbons is, in fact, bent away from the double bond midpoint reflecting the antibonding character of this MO.

C. Magnetic coupling

In the previous section the nature and the distribution of the ground-state spin density of $V(TCNE)_2$ were analyzed. It has been observed that the spin-up population is mainly localized on the V-t_{2g}^3 MOs and the spin-down population is primarily distributed over the π_z^* MOs of the two TCNEs. In this section the magnetic interactions between these localized spin units, which determine the observed macroscopic magnetic behavior, are analyzed. To accomplish this, the energies of distinct spin states corresponding to different orientations of the three spin units within the unit cell (V, equatorial $[TCNE]^{\cdot-}$, and apical $[TCNE]^{\cdot-}$) have been computed. Four different spin states, labeled as FI1, FI2, FI3, and FO, have been investigated and the corresponding energies are presented in Table III. For coupling in all the directions considered here, the antiparallel alignment of the spins in the $[TCNE]^{\cdot-}\pi^*$ states and the 3/2 spin of V^{II} is energetically favored (see Table III), in excellent agreement with the magnetic ground state deduced from susceptibility measurements.[3,12,15] The ground state, FI1, is a ferrimagnetic

TABLE III. Total magnetic moment per $V(TCNE)_2$ unit cell (S in μ_B), Mulliken spin population (in $|e|$) of the proposed spin units, and total-energy differences (ΔE_{tot} in eV/p.u.c.) with respect to the ground state ($S=1$) for the computed spin configurations. All the results are reported for the ground-state optimized geometry.

Configuration	$S(\mu_B)$	Spin unit	$\mu(\|e\|)$	ΔE_{tot}(eV/p.u.c.)
		V	+2.42	
		$[TCNE]^-_{eq}$	−0.60	
FI1	+1	$[TCNE]^-_{ap}$	−0.82	
		V	+2.54	
		$[TCNE]^-_{eq}$	+1.23	
FI2	+3	$[TCNE]^-_{ap}$	−0.77	+0.3855
		V	+2.49	
		$[TCNE]^-_{eq}$	−0.58	
FI3	+3	$[TCNE]^-_{ap}$	+1.09	+0.1894
		V	+2.60	
		$[TCNE]^-_{eq}$	+1.28	
FO	+5	$[TCNE]^-_{ap}$	+1.13	+0.6305

state with total magnetic moment equal to $1\mu_B$ per unit cell. The computed spin coupling between the $3d$ spins and the π^* spins is approximately isotropic, i.e., the strength of the magnetic interaction between the metal ion and the two different ligands is the same. The large difference in stability of the FI2 state with respect to the FI3 state is due to the different number of TCNEs coordinating the metal ion in the equatorial and apical directions, and hence the different number of nearest-neighbor units whose spin population is flipped. The spin energetics can therefore be reproduced using a simple Ising model Hamiltonian

$$\hat{H} = -4J_{eq}S_V S_{eq} - 2J_{ap}S_V S_{ap},$$

which describes the nearest-neighbor interactions of three localized magnetic moments (S_V, S_{eq}, and S_{ap}). The spin values were taken to be $S_V=+\frac{3}{2}$ and $S_{eq}=S_{ap}=-\frac{1}{2}$, which are the formal values of V^{2+} in a high spin state and of the radical anion $[TCNE]^{\cdot-}$, respectively, and are consistent with the values typically used to interpret the observed saturation magnetization.[7,8] A least-squares fit of the Hamiltonian to the energetics given in Table III has determined two magnetic coupling constants, $J_{eq}=-68.9$ meV and $J_{ap}=-72.4$ meV, with error bars of 4.6 and 9.3 meV, respectively. This simple Ising model reproduces the energies of each computed spin state (Table III) to within 10%. One of the assumptions of the nearest-neighbor Ising model is that the magnitude of the spin is not dependent on the magnetic order. The Mulliken spin population analysis indicates this condition is satisfied for the spin localized on V, μ_V, which exhibits relatively small fluctuations varying in the range of $2.42\mu_B-2.60\mu_B$. The condition is not satisfied for the spin population of both equatorial and apical TCNEs. A mean-field solution[1] of this three center Ising model yields a T_C of ~4000 K, approximately one order of magnitude greater than that deduced from susceptibility measurements for disordered $V(TCNE)_2$.[3,8,9,51] The strong suppression of the T_C from this

mean-field value may be due to an interplay of long-range disorder and thermal fluctuations.

IV. DISCUSSION

The structural model proposed here, combined with hybrid-exchange density functional theory, adequately reproduces many of the observed properties of $V(TCNE)_2$. In particular, the computed results are fully consistent with the half semiconducting behavior,[12,13] the observed saturation moment of $\sim 1\mu_B$ per formula unit,[7,8,15] and the magnetic behavior[3] displayed by the material. The high-temperature magnetic ordering is found to be a consequence of the strong nearest-neighbor magnetic coupling between the spins localized on the metal ion and the organic ligand. The essential features for strong magnetic coupling are proposed to be the formation of a three-dimensional network of V^{2+} ions and $[TCNE]^{\cdot-}$ radicals, the high degree of local order in the coordination environment of the metal ions, and the existence of hybrid d-π and d-σ states delocalized over both V's and TCNEs. These diffuse hybrid V/TCNE states, identified by analyzing the computed electronic structure, evidence a significant overlap between the V and both $[TCNE]^{\cdot-}$ ligands. The majority-spin upper valence bands correspond to V t_{2g} AOs, d_{xz}, d_{yz}, and $d_{x^2-y^2}$, hybridized with specific p AOs of TCNEs cyano carbons so that the overlap between the p and the t_{2g} lobes is maximal. Each p AO contributes up to 13% to the linear combination of atomic orbitals (LCAO) expansion of each of the delocalized states. At lower energies spin-polarized subbands related to V e_g, d_{xy}, and d_{z^2}, and TCNEs σ MOs are found. This is consistent with a recent XAS and magnetic circular dichroism (MCD) study by Kortright *et al.*,[52] who have proposed a specific covalent bonding mechanism based on the σ bonding and π backbonding models for octahedrally coordinated metal ions. These findings suggest a strong V–N σ bonding interaction resulting in the formation of a locally ordered 3D network[14] and a weaker π backbonding.

Further insight into the mechanism for magnetic coupling can be obtained by comparing the computed results of the bulk crystal with those of the isolated $[TCNE]^{\cdot-}$ ion. The Mulliken spin population of $[TCNE]^{\cdot-}$ in the $V(TCNE)_2$ crystal is considerably different to that observed for the isolated $[TCNE]^{\cdot-}$ (Table II). The significant reorganization of the spin distribution can be understood by considering the strong interaction between V^{2+} ions and $[TCNE]^{\cdot-}$ ligands. The increased delocalization of the spin-down population within the ligand and its displacement from the vinyl C's to the N's are indicative of significant exchange interactions with the antiparallel spin of the neighboring V's. The increase in the spin-up population of the cyano C's is induced by the metal ion which donates part of its $3d$ localized spin. Many of these features can be understood using a combination of spin delocalization and spin polarization[1,53] models. The spin delocalization model accounts for the observed spin-up density distribution. This is determined by the composition of the majority-spin upper valence bands, i.e., the α spin is delocalized on the V t_{2g} orbitals and the cyano C's p AOs, according to the relative weights with which these AOs contribute to these hybridized states. The spin-polarization model correctly predicts the spin distribution induced in the molecule by the α spin on the V ions. According to this mechanism, the presence of unpaired α electron on the metal ions favors the concentration of β spin on the neighboring N's. This is consistent with an extension of Lieb's theorem which applies to extended bipartite lattices.[54] This effect propagates through the molecule inducing the antiparallel alignment of π spin localized on nearest-neighbor sites (N.B. the two vinyl carbons are considered as a unique spin unit). This specific spin-density pattern, commonly observed for planar conjugated π systems such as $[TCNE]^{\cdot-}$,[1,55,56] is often referred as "the spin alternation rule" and is known to produce long-range spin polarization and mediate long-range magnetic interactions.[57–59]

The proposed model structure allows the description of the magnetic coupling between the three spin units within the unit cell (V, equatorial $[TCNE]^{\cdot-}$, and apical $[TCNE]^{\cdot-}$) in terms of a simple Ising spin Hamiltonian. The magnetic constants determined using this Hamiltonian, J_{eq} and J_{ap}, are consistent with strong antiparallel coupling between the V $3d$ and the TCNEs π^* magnetic moments, and imply a value of T_C well above room temperature. The ground state of the material is predicted to be ferrimagnetic in agreement with saturation magnetization results.[3,7,8,12] The use of B3LYP combined with mean-field (MF) Ising model would be expected to overestimate T_C by up to a factor of two, yielding a value considerably lower than that calculated here. This suggests that long-range disorder strongly affects the magnetic behavior of these compounds. It thus follows that the design of an ideal system could lead to improved materials with remarkably high transition temperatures. A detailed investigation of low-lying excited spin states corresponding to different alignments of the metal ion spins has been carried out. Suitable supercells of the fundamental cell have been created by doubling along **a**, **b**, and **c**, and have been used to study the long-range V–V exchange interactions along all the crystallographic directions. The negligible spin energetics obtained using a next-nearest-neighbor Ising Hamiltonian showed no through-space magnetic coupling between the metal ions.

V. CONCLUSIONS

A periodic model of the hybrid molecule-based $V(TCNE)_2$ magnet has been proposed, and the material structural, electronic, and magnetic properties have been simulated using hybrid-exchange density functional theory. The analysis of the computed results has shown that this model system accurately reproduces the major features of the experimental behavior of $V(TCNE)_2$. In confirmation, a fully spin-polarized half semiconducting ground state with net magnetization corresponding to one unpaired electron per formula unit has been predicted as a result of the antiparallel arrangement of the unpaired V^{2+} $3d$ spin and the two $[TCNE]^{\cdot-}\pi^*$ spins.[3,9] The magnitude (and the sign) of the magnetic coupling constants, obtained from total-energy differences computed for a set of spin configurations within a simple nearest-neighbor Ising model, has shown strong anti-

ferromagnetic coupling between the V ions and the $[TCNE]^{\cdot-}$ ligands in all the crystallographic directions. This result is consistent with the high-temperature magnetic ordering experimentally observed.[3,8,9,51] The formation of delocalized V-TCNE states and the remarkable effect of the crystal environment on the ligand valence and conduction states, and spin distribution provide further confirmation of the considerable interaction between the V and the neighboring $[TCNE]^{\cdot-}$. Finally, a detailed investigation of the computed electronic structure in terms of electronic band structure, Mulliken spin populations, and spin-density maps has given useful insight into the physical origin of the exceptional magnetic behavior of $V(TCNE)_2$.

ACKNOWLEDGMENTS

G.D.F. would like to thank the STFC for strategic initiative grant, the EPSRC-GB for provision of computer time under the Materials Chemistry Consortium Project No. GR/S13422/01, and also G. Mallia for technical assistance and useful discussions.

[1] J. S. Miller and A. J. Epstein, Angew. Chem., Int. Ed. Engl. **33**, 385 (1994), and references therein.
[2] J. S. Miller and A. J. Epstein, MRS Bull. **25**, 21 (2000), and references therein.
[3] J. M. Manriquez, G. T. Yee, R. S. McLean, A. J. Epstein, and J. S. Miller, Science **252**, 1415 (1991).
[4] C. M. Wynn, M. A. Girtu, J. Zhang, J. S. Miller, and A. J. Epstein, Phys. Rev. B **58**, 8508 (1998).
[5] M. A. GîrŢu, C. M. Wynn, J. Zhang, J. S. Miller, and A. J. Epstein, Phys. Rev. B **61**, 492 (2000).
[6] D. de Caro, M. Basso-Bert, J. Sakah, H. Casellas, J.-P. Legros, L. Valade, and P. Cassoux, Chem. Mater. **12**, 587 (2000).
[7] K. I. Pokhodnya, A. J. Epstein, and J. S. Miller, Adv. Mater. (Weinheim, Ger.) **12**, 410 (2000).
[8] J. S. Miller and A. J. Epstein, Chem. Commun. **1998**, 1319, and references therein.
[9] K. I. Pokhodnya, D. Pejakovic, A. J. Epstein, and J. S. Miller, Phys. Rev. B **63**, 174408 (2001).
[10] M. P. de Jong, C. Tengstedt, A. Kanciurzewska, E. Carlegrim, W. R. Salaneck, and M. Fahlman, Phys. Rev. B **75**, 064407 (2007).
[11] D. de Caro, C. Faulmann, and L. Valade, Chem.-Eur. J. **13**, 1650 (2007).
[12] V. N. Prigodin, P. R. Nandyala, K. I. Pokhodnya, J. S. Miller, and A. J. Epstein, Adv. Mater. (Weinheim, Ger.) **14**, 1230 (2002).
[13] N. P. Raju, T. Savrin, V. N. Prigodin, K. I. Pokhodnya, J. S. Miller, and A. J. Epstein, J. Appl. Phys. **93**, 6799 (2003).
[14] D. Haskel, Z. Islam, J. Lang, C. Kmety, G. Srajer, K. I. Pokhodnya, A. J. Epstein, and J. S. Miller, Phys. Rev. B **70**, 054422 (2004).
[15] V. N. Prigodin, N. P. Raju, K. I. Pokhodnya, J. S. Miller, and A. J. Epstein, Synth. Met. **135-136**, 87 (2003).
[16] S. A. Wolf, D. D. Awschalom, R. A. Buhrman, J. M. Daughton, S. von Molnár, M. L. Roukes, A. Y. Chtchelkanove, and D. M. Treger, Science **294**, 1488 (2001).
[17] H. Ohno, Science **281**, 951 (1998).
[18] T. Dietl, H. Ohno, F. Matsukura, J. Cibert, and D. Ferrand, Science **287**, 1019 (2000).
[19] C. Felser, G. H. Fecher, and B. Balke, Angew. Chem., Int. Ed. **46**, 668 (2007).
[20] J. S. Miller and A. J. Epstein, CHEMTECH **21**, 168 (1991).
[21] J. S. Miller, Adv. Mater. (Weinheim, Ger.) **6**, 322 (1994).
[22] B. G. Morin, C. Hahm, A. J. Epstein, and J. S. Miller, J. Appl. Phys. **75**, 5782 (1994).
[23] J.-W. Yoo, R. S. Edelstein, D. M. Lincoln, N. P. Raju, C. Xia, K. I. Pokhodnya, J. S. Miller, and A. J. Epstein, Phys. Rev. Lett. **97**, 247205 (2006).
[24] J.-W. Yoo, R. S. Edelstein, N. P. Raju, D. M. Lincoln, and A. J. Epstein, J. Appl. Phys. **103**, 07B912 (2008).
[25] J. Zhang, P. Zhou, W. B. Brinckerhoff, A. J. Epstein, C. Vazquez, R. S. McLean, and J. S. Miller, ACS Symp. Ser. **644**, 311 (1996).
[26] C. Tengstedt, M. P. de Jong, A. Kanciurzewska, E. Carlegrim, and M. Fahlman, Phys. Rev. Lett. **96**, 057209 (2006).
[27] E. Carlegrim, A. Kanciurzewska, P. Nordblad, and M. Fahlman, Appl. Phys. Lett. **92**, 163308 (2008).
[28] J. S. Miller, Inorg. Chem. **39**, 4392 (2000), and references therein.
[29] J.-H. Her, P. W. Stephens, K. I. Pokhodnya, M. Bonner, and J. S. Miller, Angew. Chem., Int. Ed. **46**, 1521 (2007).
[30] A. L. Tchougréeff and R. Dronskowski, J. Comput. Chem. **29**, 2220 (2008).
[31] J. S. Miller, Angew. Chem., Int. Ed. **45**, 2508 (2006).
[32] A. Zheludev, A. Grand, E. Ressouche, J. Schweizer, B. G. Morin, A. J. Epstein, D. A. Dixon, and J. S. Miller, J. Am. Chem. Soc. **116**, 7243 (1994).
[33] A. D. Becke, Phys. Rev. A **38**, 3098 (1988).
[34] A. D. Becke, J. Chem. Phys. **98**, 5648 (1993).
[35] C. Lee, W. Yang, and R. G. Parr, Phys. Rev. B **37**, 785 (1988).
[36] R. Dovesi *et al.*, *CRYSTAL06*, (Università di Torino, Torino, 2006).
[37] W. E. Pickett, Rev. Mod. Phys. **61**, 433 (1989).
[38] W. C. Mackrodt, N. M. Harrison, V. R. Saunders, N. L. Allan, M. D. Towler, E. Apra, and R. Dovesi, Philos. Mag. A **68**, 653 (1993).
[39] J. Muscat, A. Wander, and N. M. Harrison, Chem. Phys. Lett. **342**, 397 (2001).
[40] R. L. Martin and F. Illas, Phys. Rev. Lett. **79**, 1539 (1997).
[41] T. Bredow and A. R. Gerson, Phys. Rev. B **61**, 5194 (2000).
[42] I. de P. R. Moreira, F. Illas, and R. L. Martin, Phys. Rev. B **65**, 155102 (2002).
[43] J. K. Perry, J. Tahir-Kheli, and W. A. Goddard, Phys. Rev. B **63**, 144510 (2001).
[44] X.-B. Feng and N. M. Harrison, Phys. Rev. B **70**, 092402 (2004).
[45] J. Ribas-Ariño, J. J. Novoa, and J. S. Miller, J. Mater. Chem. **16**, 2600 (2006).
[46] R. Dovesi *et al.*, *CRYSTAL06 User's Manual* (Università di Torino, Torino, 2006).

[47] See http://www.crystal.unito.it/Basis_Sets/Ptable.html.
[48] H. J. Monkhorst and J. D. Pack, Phys. Rev. B **13**, 5188 (1976).
[49] E. Carlegrim, B. Gao, A. Kanciurzewska, M. P. de Jong, Z. Wu, Y. Luo, and M. Fahlman, Phys. Rev. B **77**, 054420 (2008).
[50] E. Ruiz, J. Cirera, and S. Alvarez, Coord. Chem. Rev. **249**, 2649 (2005), and references therein.
[51] A. J. Epstein and J. S. Miller, Mol. Cryst. Liq. Cryst. Sci. Technol., Sect. A **233**, 171 (1993).
[52] J. B. Kortright, D. M. Lincoln, R. S. Edelstein, and A. J. Epstein, Phys. Rev. Lett. **100**, 257204 (2008).
[53] J. S. Miller and M. Drillon, *Magnetism: Molecules to Materials* (Wiley-VCH, Weinheim, 2001), Vol. 1-3.
[54] E. H. Lieb, Phys. Rev. Lett. **62**, 1201 (1989).
[55] A. A. Ovchinnikov, Theor. Chim. Acta **47**, 297 (1978).
[56] O. Kahn, *Molecular Magnetism* (Wiley-VCH, Weinheim, 1993), and references therein.
[57] J. Chan, B. Montanari, W.-L. Chan, and N. M. Harrison, Mol. Phys. **103**, 2573 (2005).
[58] L. Pisani, J. A. Chan, B. Montanari, and N. M. Harrison, Phys. Rev. B **75**, 064418 (2007).
[59] L. Pisani, B. Montanari, and N. M. Harrison, New J. Phys. **10**, 033002 (2008).